Published in final edited form as:

ACS Biomater Sci Eng. 2018 April 9; 4(4): 1251–1264. doi:10.1021/acsbiomaterials.6b00804.

Drug-Free ROS Sponge Polymeric Microspheres Reduce Tissue Damage from Ischemic and Mechanical Injury

Kristin P. O'Grady[†,‡], **Taylor E. Kavanaugh**[†,‡], **Hongsik Cho**[†,§], **Hanrong Ye**[‡], **Mukesh K. Gupta**[‡], **Megan C. Madonna**[‡], **Jinjoo Lee**[‡], **Christine M. O'Brien**[‡], **Melissa C. Skala**[‡,⊥], **Karen A. Hasty**[§], and **Craig L. Duvall**[*,‡]

[‡]Biomedical Engineering, Vanderbilt University, 1225 Stevenson Center Lane, 5824 Stevenson Center, Nashville, Tennessee 37235, United States

[§]Orthopaedic Surgery and Biomedical Engineering, University of Tennessee Health Science Center, Research Service 151, VA Medical Center, 1030 Jefferson Avenue, Memphis, Tennessee 38104, United States

Abstract

The inherent antioxidant function of poly(propylene sulfide) (PPS) microspheres (MS) was dissected for different reactive oxygen species (ROS), and therapeutic benefits of PPS-MS were explored in models of diabetic peripheral arterial disease (PAD) and mechanically induced post-traumatic osteoarthritis (PTOA). PPS-MS (~1 μm diameter) significantly scavenged hydrogen peroxide (H_2O_2), hypochlorite, and peroxynitrite but not superoxide in vitro in cell-free and cell-based assays. Elevated ROS levels (specifically H_2O_2) were confirmed in both a mouse model of diabetic PAD and in a mouse model of PTOA, with greater than 5- and 2-fold increases in H_2O_2, respectively. PPS-MS treatment functionally improved recovery from hind limb ischemia based on ~15–25% increases in hemoglobin saturation and perfusion in the footpads as well as earlier remodeling of vessels in the proximal limb. In the PTOA model, PPS-MS reduced matrix metalloproteinase (MMP) activity by 30% and mitigated the resultant articular cartilage damage. These results suggest that local delivery of PPS-MS at sites of injury-induced inflammation improves the vascular response to ischemic injury in the setting of chronic hyperglycemia and reduces articular cartilage destruction following joint trauma. These results motivate further exploration of PPS as a stand-alone, locally sustained antioxidant therapy and as a material for microsphere-based, sustained local drug delivery to inflamed tissues at risk of ROS damage.

[*]**Corresponding Author:** craig.duvall@vanderbilt.edu. Address: Biomedical Engineering, Vanderbilt University, 5824 Stevenson Center, PMB 351631, 2301 Vanderbilt Place, Nashville, TN 37235-1631, USA.

[⊥]**Present Address**

M.C.S. is currently at Morgridge Institute for Research and Department of Biomedical Engineering, University of Wisconsin–Madison

[†]**Author Contributions**

K.P.O., T.E.K., and H.C. contributed equally. The manuscript was written through contributions of all authors. All authors have given approval to the final version of the manuscript.

Supporting Information

The Supporting Information is available free of charge on the ACS Publications website at DOI: 10.1021/acsbiomaterials.6b00804.

ORCID

Taylor E. Kavanaugh: 0000-0002-8798-2670

Notes

The authors declare no competing financial interest.

Graphical abstract

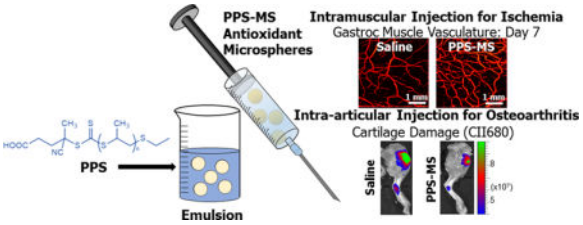

Keywords

reactive oxygen species; inflammation; osteoarthritis; diabetes; peripheral arterial disease; microspheres

1. INTRODUCTION

Reactive oxygen species (ROS) are an important aspect of normal cell growth and metabolism, but when oxidant levels exceed that of cellular antioxidant potential, tissue-damaging oxidative stress occurs.[1] Some key ROS are hydrogen peroxide (H_2O_2), hydroxyl radicals ($OH^{\cdot}$), hypochlorous acid (HOCl), and superoxide anions (O_2^{-}). Reactive nitrogen species such as nitric oxide ($NO^{\cdot}$) and highly reactive peroxynitrite anion ($ONOO^{-}$) are also important reactive species that impact pathogenesis of chronic inflammatory diseases. Oxidants can be generated exogenously (e.g., by ultraviolet light) or produced intracellularly through cytosolic enzyme systems such as NADPH oxidases (NOX) and uncoupled nitric oxide synthase (NOS), and through normal metabolism in mitochondria and peroxisomes. ROS levels are kept in balance through an enzymatic antioxidant defense system composed of superoxide dismutase, catalase, glutathione peroxidase, and peroxiredoxins in combination with nonenzymatic scavengers such as flavonoids and glutathione. If ROS levels are too low, cellular proliferation and host defense against microbial invasion are impaired, while excessive ROS can cause cell and tissue damage and activate inflammatory signaling pathways. $OH^{\cdot}$ is capable of oxidizing most biological molecules, and O_2^{-} can either react directly with biomolecules or produce other ROS (H_2O_2 and $OH^{\cdot}$).[2] H_2O_2 is not highly reactive itself, but it is an intermediate to both $OH^{\cdot}$ and hypochlorite (^{-}OCl) radical production.[3] Similarly, $NO^{\cdot}$ alone is not very reactive to nonradical species, but it can generate other reactive nitrogen species or combine with O_2^{-} to form the strongly reactive $ONOO^{-}$. Excessive production of these ROS exacerbates many inflammation-associated diseases through DNA damage, protein modification, lipid peroxidation, disruption of cell signaling, and causing cell death. These consequences of oxidative stress make ROS a potentially valuable therapeutic target for diseases such as diabetic peripheral arterial disease (PAD) and post-traumatic osteoarthritis (PTOA) whose progression is tightly tied to oxidative stress.[4–9]

PAD is a common comorbidity of diabetes,[7,8] with oxidative stress providing a key link between diabetes and vascular dysfunction.[8,10] There are several mechanistic connections between diabetic vascular dysfunction and oxidative stress. The function of endothelial progenitor cells needed for vasculogenesis is damaged by chronic oxidative stress[11] as are

many intracellular signaling pathways. Post-translational modification of extracellular-signal-regulated kinase-5 (ERK5) by H_2O_2 impairs its anti-inflammatory activity in endothelial cells.[12] Excess O_2^- can modify and impair the function of the transcription factor hypoxia-inducible factor 1 (HIF-1), negatively affecting signaling pathways critical to vasculogenesis.[13] Increased levels of O_2^- also contribute to decreased bioavailability of endothelium-derived $NO^·$ because of its reaction with O_2^-, forming the strong and cytotoxic oxidant $ONOO^-$.[14] $ONOO^-$ has significant, negative roles in endothelial dysfunction, loss of endothelial NO synthase (eNOS) activity, and downstream generation of additional ROS.[14–16] Because of the complexity of the pathways through which diabetes impairs angiogenesis and arteriogenesis, it is logical to pursue new PAD therapies that target an upstream factor such as overproduction of ROS.

In PTOA, osteoarthritis develops following joint injuries such as dislocation, ligament/meniscal tears, and fractures that trigger inflammation. The presence of lipid peroxidation products and nitrotyrosine in biological fluids and tissue of patients with OA suggests that ROS play a role in cartilage degradation and may be a viable therapeutic target.[17,18] The role of ROS in PTOA progression is also supported by the observation that chondrocytes in articular cartilage produce abnormal levels of ROS in response to mechanical stress and to stimulation with inflammatory cytokines and chemokines, as well as lipid-derived inflammatory mediators.[19,20] In addition to classical signaling molecules, chondrocytes produce inflammation-propagating ROS such as $NO^·$ and O_2^-,[21] which in turn generate derivative radicals including $ONOO^-$, H_2O_2, and ^-OCl.[5] Recent studies highlight the importance of H_2O_2 in the onset of OA,[22] where high levels of H_2O_2 cause the hyperoxidation of peroxiredoxins, which inhibits peroxiredoxin antioxidant function and exacerbates ROS-induced tissue damage. Oxidative stress can contribute to PTOA by driving breakdown of extracellular components such as proteoglycans and collagens by increasing production of proteases[19,20] as well as the direct depolymerization of hyaluronic acid. In the setting of OA, ROS are also utilized as a "secondary messenger" in proinflammatory signaling pathways; for example, excessive ROS, in particular H_2O_2, can result in the formation of cysteine sulfenic acid residues (Cys-SOH). Cys-SOH can lead to production of cartilage-damaging matrix metalloproteinase (MMP)-13 through the oxidation/reduction of cysteines involved in the MAP kinase JNK-2 pathway.[21] The role of ROS in many inflammatory pathways that propagate PTOA has been confirmed, which indicates the potential for therapeutic scavenging of ROS to halt PTOA progression.

One approach to alleviating oxidative stress is delivery of the recombinant form or synthetic analogs of endogenous antioxidant enzymes such as catalase and superoxide dismutase which detoxify H_2O_2 and O_2^-, respectively. For example, preclinical studies have demonstrated improvement of vascular function and response to ischemia through treatment with catalase and superoxide dismutase (SOD) mimetics in models with elevated ROS production.[13,23–25] However, these antioxidant treatments are often administered via systemic injection or in drinking water, which requires multiple administrations. Sustained delivery depots may be more effective, convenient, and safe for patients with localized disease such as PAD and PTOA, and will help to minimize off-target effects that can occur such as impairment of the mitochondrial electron transport chain in healthy tissues.[26,27] Several particle-based systems have been employed to improve delivery of native SOD and

catalase enzymes[28–32] including a hybrid system consisting of SOD conjugated to polysulfide-containing micelles.[33] Recently, polymeric systems including nanoparticles,[34] hydrogels,[26] and pH-responsive microparticles have been employed for delivery of nitroxide radicals that mimic the function of SOD in scavenging O_2^-.[35]

Previously, we demonstrated the utility of an ROS-responsive, H_2O_2-scavenging microsphere system for delivery of hydrophobic drugs such as the anti-inflammatory and antioxidant molecule curcumin from a local depot (Figure S1).[36] This system is based on poly(propylene sulfide) (PPS), which undergoes a phase change from a hydrophobic to a hydrophilic state upon oxidation,[37] permitting on-demand release of encapsulated drug.[38,39] Blank PPS microspheres (PPS-MS) containing no drug scavenged ROS in vitro (Figure S1A) and in ischemic muscle (Figure S1B), although unloaded PPS-MS did not functionally improve the vascular response to ischemia in young mice with short-term hyperglycemia.[36] The antioxidant properties of PPS have also been explored in a hydrogel formulation, where PPS served as an ROS sink and protected cells from cytotoxic levels of H_2O_2.[39] In the present work, we more comprehensively define the antioxidant properties of PPS for a range of ROS types and therapeutically test blank PPS-MS in a more severe, long-term diabetic animal model of PAD and a model of mechanically induced PTOA.

2. MATERIALS AND METHODS

2.1. Materials

All chemicals were purchased from Sigma-Aldrich (St. Louis, MO, USA) except the following. Propylene sulfide (>96%) was purchased from Acros Organics through Fisher Scientific (Pittsburgh, PA, USA) and was purified by distillation over CaH_2 powder just before polymerization. Amplex Red Hydrogen Peroxide/Peroxidase Assay kit was purchased from Thermo Fisher Scientific (Molecular Probes, Waltham, MA, USA). Peroxynitrite was purchased as a solution in 0.3 M sodium hydroxide from Cayman Chemical (Ann Arbor, MI, USA). Amplite Fluorimetric Hypochlorite Assay kit was purchased from AAT Bioquest (Sunnyvale, CA, USA). Hypochlorite Detection Kit was purchased from Cell Technology (Fremont, CA 94538). Nitric Oxide Assay Kit (Colorimetric) was purchased from Abcam (Cambridge, MA, USA). Promega Celltiter Glo Luminescent Cell Viability Assay Kit was purchased from Fisher Scientific.

2.2. Microsphere Synthesis

2.2.1. Synthesis of Poly(propylene sulfide) (PPS)—PPS was prepared as previously described[39] by anionic ring opening polymerization of propylene sulfide using DBU/1-buthanethiol. Briefly, in a hot air-dried and nitrogen flushed 100 mL flask, 1,8-diazabicyclo[5.4.0]undec-7-ene (DBU) (4.5 mmol, 0.673 mL) in dry tetrahydrofuran (THF) (25 mL) was degassed for 30 min, and the reaction mixture was cooled to 0 °C. To this flask was added dropwise a previously degassed solution (30 min) of 1-butanethiol (1.5 mmol, 0.161 mL) in THF (20 mL), and the solution was allowed to react for 30 min. Later, freshly distilled and degassed propylene sulfide (120 mmol, 9.39 mL) was added to the reaction mixture, and the temperature was maintained at 0 °C for 30 min. The polymerization was carried out for another 1.5 h at room temperature and quenched by addition of 2-iodoethanol

(2 mmol, 0.40 g). On the next day, the polymerization mixture was filtered to remove precipitated salt, and the filtered polymer solution was concentrated under vacuum. The crude polymer in dichloromethane (5 mL) was purified by three precipitations into cold methanol and dried under high vacuum to yield a colorless viscous polymer. ^{1}H NMR (400 MHz; $CDCl_3$, δ): = 1.3–1.4 (s, CH_3), 2.5–2.8 (s, −CH), 2.8–3.1 (s, CH_2), 3.72 (t, CH_2−OH).

2.2.2. Characterization of PPS—PPS was characterized for structure, molecular weight, and polydispersity as described previously.[36,39] The number-average molecular weight (M_n) and polydispersity (PDI) of PPS were assessed by gel permeation chromatography (GPC, Agilent Technologies, Santa Clara, CA, USA) using dimethylformamide (DMF) + 0.1 M lithium bromide mobile phase at 60 °C through three serial Tosoh Biosciences TSKGel Alpha columns (Tokyo, Japan). An Agilent refractive index (RI) and Wyatt miniDAWN TREOS light scattering (LS) detector (Wyatt Technology Corp., Santa Barabara, CA, USA) were used to calculate absolute molecular weight based on dn/dc values experimentally determined through a refractometer. The chemical structure of the PPS was confirmed by ^{1}H nuclear magnetic resonance (NMR) recorded in $CDCl_3$ with a Brüker 400 MHz spectrometer.

2.2.3. Microsphere Fabrication and Characterization—PPS-MS were prepared using the oil-in-water (O/W) emulsion solvent evaporation method[40,41] as described previously.[36] Briefly, PPS (60 mg) was ultrasonicated (Cole-Parmer, USA) in chloroform (1 mL) until completely dissolved to form the oil (O) phase. The O phase was then added dropwise into 1% (w/v) aqueous poly(vinyl alcohol) (PVA) solution (7 mL) and emulsified using an Ultra-Turrax TP 18–10 homogenizer (Janke and Kunkel KG, IKA-WERK) at 20,000 rpm for 1 min. The emulsion was transferred to a round-bottom flask and subjected to high vacuum (~635 mmHg) using a rotary evaporator (Rotavapor RII, BUCHI, Switzerland) for 1 h to remove the chloroform. Microspheres were then recovered by centrifuging the remaining aqueous solution at 7500xg for 8 min. The microspheres were then washed once with deionized water to remove excess PVA. Lastly, the microspheres were lyophilized (Labconco Freezone 4.5, USA) prior to storage. Microspheres were characterized for size and morphology by scanning electron microscopy (SEM, Hitachi S-4200, Hitachi Ltd., Tokyo, Japan). The microspheres were suspended in a water drop and placed on a double sided carbon tape attached to an aluminum stub, air-dried, then sputter-coated with gold for 60 s. Microsphere size was quantified from SEM images using ImageJ 1.43u software (Freeware, NIH, Bethesda, MD) to measure the diameter of >600 microspheres.

2.3. Degradation and ROS Scavenging Activity of PPS in Vitro

2.3.1. PPS Degradation by ROS in Vitro—The degradation of PPS with various ROS was characterized using GPC. PPS was dissolved in a solution of THF and diH_2O (50/50) at a concentration of 10 mg/mL. H_2O_2, $^-$OCl, and SIN-1 were added to polymer solutions at various concentrations. ROS-treated PPS samples were incubated 24 h on a shaker at 37 °C. ROS-treated PPS samples were then lyophilized and dissolved in DMF + 0.1 M lithium bromide. Samples were filtered and assessed by GPC using the system described above. Further ^{1}H NMR characterization of the treated PPS samples was performed with a Brüker

400 MHz spectrometer after the samples were lyophilized and reconstituted in $CDCl_3$. PPS and oxidized PPS peaks were quantified based on previous literature.[38] Percent oxidized PPS was quantified and used to determine the ROS concentration that resulted in oxidation of 50% of the polymer, or "oxidant concentration 50" (OC50).

2.3.2. PPS-MS Degradation by ROS in Vitro—Degradation of PPS-MS with exposure to different ROS was visualized using microscopy. PPS-MS were suspended at a concentration of 1 mg/mL in PBS in chambered cover glass. Microsphere samples were incubated with PBS, 1250 mM H_2O_2, 500 mM NaOCl, or 50 mM SIN-1 for 24 h at 37 °C. Following this incubation, microspheres were visualized using microscopy on a Nikon Eclipse Ti inverted microscope (Nikon Instruments Inc., Melville, NY).

2.3.3. Hydrogen Peroxide Scavenging in Vitro—H_2O_2-scavenging activity of the PPS-MS was verified in vitro using an Amplex Red Hydrogen Peroxide/Peroxidase Assay kit from Thermo Fisher Scientific (Molecular Probes, Waltham, MA, USA) according to the manufacturer's instructions. One hundred microliters H_2O_2 was prepared as the reaction solution. H_2O_2 was added to wells in a black-walled, 96-well plate containing either PBS or PPS-MS (final PPS-MS concentration ranging from 0.25 to 1.5 mg/mL). The samples were incubated at 37 °C for 1 week, a time scale previously shown to be appropriate for the reaction of PPS with H_2O_2.[37] The Amplex Red working solution was freshly prepared as described by the manufacturer using the included Amplex Red, horseradish peroxidase, and 1× reaction buffer. The working solution was added to the wells, and fluorescence was measured in a plate reader at 30 min with an excitation of 530 nm and an emission of 590 nm.

2.3.4. Peroxynitrite Scavenging in Vitro—The ability of PPS-MS to scavenge $ONOO^-$ was tested in vitro using a Pyrogallol Red (PGR) bleaching assay.[42] Treatment groups consisting of PBS, PPS-MS (0.5–1.5 mg/mL), and ascorbic acid (positive control, pH adjusted to 7.4) were prepared in a 48-well plate with 500 μL volume per well. A PGR stock solution was prepared in PBS (0.025 μM), and 10 μL was added to each well. $ONOO^-$ stock solution was thawed on ice and diluted to a concentration of 1 mM in 0.3 M NaOH. After baseline absorbance of the dye was measured in a plate reader at 540 nm, 5 μL of $ONOO^-$ was added to each well (final concentration of 10 μM) and absorbance measurements began immediately and were collected for 1 h.

2.3.5. Hypochlorite Scavenging in Vitro—PPS-MS scavenging of ^-OCl was measured in vitro using a fluorimetric ^-OCl assay kit. One hundred microliters of PPS-MS in PBS were added to a 96-well plate at various concentrations ranging from 0.25 to 1 mg/mL. One hundred microliters of 10 mM NaOCl was added to wells containing PPS-MS or PBS. The plate was incubated for 10 min at 25 °C on a shaker. Following the incubation, 50 μL of each solution was transferred to a black-walled 96-well plate. Fifty microliters of ^-OCl assay mixture (200 × Oxirite Hypochlorite Sensor +5 mL Assay Buffer) was added to each well. Fluorescence intensity in the wells was measured in a plate reader with an excitation of 540 nm and an emission of 590 nm.

2.3.6. Nitrite Scavenging in Vitro—PPS-MS scavenging of nitrite was measured in vitro using a colorimetric nitric oxide assay kit. Eighty-five microliters of 1 mg/mL PPS-MS in PBS was added to a 96-well plate. Five nmol nitrite was added to wells containing PPS-MS or PBS. The plate was incubated at room temperature for 1 h. Five microliters of enhancer was added to all wells followed by the addition of 50 μL of Griess Reagent 1 and 50 μL of Greiss Reagent 2. Absorbance was immediately measured at 540 nm.

2.3.7. Superoxide Scavenging in Vitro—In vitro O_2^- scavenging activity of the PPS-MS was evaluated using a dihydroethidium (DHE) fluorescence assay. The scavenging of O_2^- by PPS-MS (1, 0.5, and 0.1 mg/mL) was investigated using an O_2^--generating, cell-free enzymatic system containing 0.046 U/ml xanthine oxidase (XO) and 0.2 mM xanthine (X) in a black-walled, 96-well plate containing 10 μM DHE (final concentration). The fluorescence intensity was measured in a plate reader (Tecan Group Ltd., Mannedorf, Switzerland) over a time frame of 1.5 h with an excitation of 405 nm and an emission of 570 nm. The reaction of DHE with O_2^- forms a specific fluorescent product, 2-OH-ethidium (2OH-E), and the selected excitation/emission wavelengths provide optimal specificity for measuring O_2^-.[43,44] Specificity of the assay for O_2^- detection was confirmed using bovine SOD (20 U/mL) as a positive control treatment in a well containing X/XO and DHE.

2.4. PPS-MS Scavenging of ROS in Vitro in LPS-Stimulated Macrophages

2.4.1. PPS-MS Scavenging of Cellular Hydrogen Peroxide—RAW 264.7 cells were seeded at 500,000 cells/well in 24-well plates in phenol red-free DMEM supplemented with 10% FBS and ciprofloxacin and were allowed to adhere overnight. Cells were treated for 1 h with PPS-MS in fresh DMEM, and 1 μg/mL of LPS was then added prior to an additional 24 h of incubation. Control groups consisted of cells without LPS stimulation and stimulated cells with no microsphere treatment. After 24 h of stimulation, 50 μL of cell supernatant was collected and H_2O_2 levels were measured with an Amplex Red assay using the manufacturer's instructions as described above.

2.4.2. PPS-MS Scavenging of Cellular Hypochlorite, Hydroxyl Radicals, And Peroxynitrite—RAW 264.7 cells were seeded at 50,000 cells/well in 96-well plates in phenol red-free DMEM supplemented with 10% FBS and ciprofloxacin and were allowed to adhere overnight. Cells were treated for 1 h with PPS-MS in fresh DMEM, and 1 μg/mL of LPS was added prior to an additional 24 h of incubation. Control groups consisted of cells without LPS stimulation and stimulated cells with no microsphere treatment. After 24 h of stimulation, cells were washed with PBS and then incubated with 5 mM aminophenyl fluorescein (APF) in phenol red-free, serum-free DMEM for 25 min. Cells were washed with PBS, and fresh phenol red-free, serum-free DMEM was added to the cells. APF intracellular fluorescence (linked with presence of ^-OCl, $OH^·$, and $ONOO^-$) was measured on a plate reader at 30 min following media exchange (Ex/Em 488/550 nm).

2.4.3. PPS-MS Scavenging of Multiple Cellular ROS—RAW 264.7 cells were seeded at 75,000 cells/well in 12-well plates in DMEM supplemented with 10% FBS and ciprofloxacin and were allowed to adhere overnight. Cells were treated for 1 h with PPS-MS in fresh DMEM medium, and 1 μg/mL of LPS was then added prior to an additional 24 h of

incubation. Control groups consisted of cells without LPS stimulation and stimulated cells with no microsphere treatment. After 24 h of stimulation, cells were washed with PBS and then incubated with 5 μM H2-DCFDA in phenol-red free, serum-free DMEM for 25 min. Cells were washed with PBS and harvested in PBS. Intracellular fluorescence, which corresponds to levels of $ONOO^-$, $OH^·$, and several other ROS,[45] was measured via flow cytometry (FACSCalibur, BD Biosciences) and analyzed using FlowJo software.

2.4.4. PPS-MS Cytotoxicity—RAW 264.7 cells were seeded at 50,000 cells/well in a 96-well plate in DMEM supplemented with 10% FBS and ciprofloxacin and allowed to adhere overnight. Cells were treated for 24 h with PPS-MS in fresh DMEM. Cells were washed once with PBS +/+. One hundred microliters of PBS +/+ was added to all wells followed by the addition of 100 μL of CellTiter-Glo reagent prepared according to the manufacturer's instructions. The plate was mixed on a shaker at room temperature for 2 min, incubated at room temperature for 10 min, and then read for luminescence using IVIS (Lumina Series III, PerkinElmer) imaging.

2.5. In Vivo Experiments

2.5.1. Diabetes Model Development—Two variations on a Type 1 diabetes model were assessed prior to selecting the model for the therapeutic studies. In both variations, male FVB mice (Jackson Laboratory) were given daily intraperitoneal injections of streptozotocin (STZ, 50 mg/kg) for 5 consecutive days after a 5 h fast.[46] The first group was given STZ at 9 weeks of age and was hyperglycemic for 5 weeks prior to surgical induction of ischemia. The second group was also given STZ at 9 weeks of age, but surgery was delayed until 15 weeks of hyperglycemia to assess the effects of more chronic hyperglycemia and advanced age, characteristics that are more representative of diabetic PAD in humans. The two groups are respectively referred to as the "younger cohort–5 weeks diabetic" and "older cohort–15 weeks diabetic". Nondiabetic mice that were age-matched to the younger and older cohorts at the time of surgery were included to assess the effects of hyperglycemia in each variation of the model. In all groups, glucose levels were measured at the onset of hyperglycemia following the STZ treatment and again at the time of surgery. Mice with glucose levels consistently above 300 mg/dL were considered diabetic.

2.5.2. Mouse Hind Limb Ischemia Model—After 5 or 15 weeks of hyperglycemia, hind limb ischemia (HLI)[47] was surgically induced in diabetic and age-matched nondiabetic mice as described previously.[36] Briefly, the femoral artery and vein of the right hind limb were ligated with 6–0 sutures proximal to the origins of the superficial epigastric artery and deep branch of the femoral artery and at a distal site, proximal to the vessels that branch from the femoral artery near the knee. Major side branches were also ligated with 6–0 sutures before the ligated segment of the femoral artery and vein was excised. The incision was closed with interrupted 5–0 nylon sutures. In therapeutic experiments, treatments were injected intramuscularly in the ischemic limb immediately following closure of the skin incision. Treatment injections ($n = 20$ mice received saline, $n = 17$ mice received 1.2 mg of PPS microspheres) were administered in a total volume of 100 μL divided among 3 injection sites in the adductor muscle and 3 injection sites in the gastrocnemius muscle in order to treat the entire ischemic region. Surgery was performed under isoflurane anesthesia at

normal body temperature. Analgesia was administered subcutaneously preoperatively and every 24 h postoperatively until animals exhibited normal appearance and behavior (5–10 mg/kg ketoprofen). Mice were fed a standard chow diet ad libitum with free access to water. All diabetes and HLI protocols were approved by the Institutional Animal Care and Use Committee of Vanderbilt University and done in accordance with the National Institute of Health's Guide for the Care and Use of Laboratory Animals.

2.5.3. ROS Measurement in Extracted Muscle Tissue—After 14 days of HLI, the gastrocnemius muscles were extracted immediately postmortem, and dissected pieces of tissue were weighed and transferred into Krebs HEPES Buffer (pH 7.35) on ice. Amplex Red working solution was prepared using components from the Molecular Probes Amplex Red Hydrogen Peroxide/Peroxidase Assay kit as follows: 1 vial of Amplex Red (154 μg) was dissolved in 60 μL DMSO and added to 11.82 mL of Krebs HEPES Buffer along with 120 μL of horseradish peroxidase (from a stock solution of 10 U/ml in 0.05 M sodium phosphate at pH 7.4). Three hundred microliters of working solution was added to each well in a 48-well plate. Tissue samples were transferred into the Amplex Red solution and incubated in the dark for 1 h at 37 °C. Tissue samples weighing approximately 20 mg were used to ensure H_2O_2 diffusion out of the tissue. A series of dilutions of H_2O_2 from 15 μM to 0 μM was prepared in a black-walled 96-well plate at the same time that the tissue incubation began. After 1 h, 150 μL of solution from each sample was transferred to the black 96-well plate, and Amplex Red fluorescence was measured on an IVIS imaging system (Lumina Series III, PerkinElmer) with 530/590 nm excitation/emission filters. Tissue hydrogen peroxide concentration was normalized to tissue mass, and ischemic limb values were normalized to the contralateral control muscle for each animal (n = 4–5 mice/group).

2.5.4. Hyperspectral Imaging of Hemoglobin Oxygen Saturation in HLI—Hemoglobin oxygen saturation (HbSat) was measured in the footpads of the hind limbs using hyperspectral imaging as described previously[36,48] at days 0, 3, 7, 14, 21, and 28 postsurgery. Briefly, diffuse reflectance images were collected in the visible light range from 500 to 620 nm in 8 nm increments using a liquid crystal tunable filter (CRi, Inc.) mounted on a cooled CCD camera (Andor, 1392 × 1040 pixel) with a variable focal length camera lens (Navitar, f = 18–108 mm). Illumination was provided by a halogen lamp. HbSat was calculated for each image pixel using a modified version of Beer's law.[48–50] Average HbSat values were computed for each footpad, and the ischemic footpad HbSat was normalized to that of the contralateral footpad for each animal.

2.5.5. Perfusion Imaging in HLI—Perfusion images of the footpads were acquired at days 0, 3, 7, 14, 21, and 28 postsurgery with a laser Doppler perfusion imager (LDPI) (Perimed PeriScan PIM II). An average perfusion value was computed for each footpad, and the ischemic footpad perfusion was normalized to that of the contralateral footpad for each animal.

2.5.6. Intravital Imaging of Vascular Remodeling in HLI with Optical Coherence Tomography—At 0, 3, 7, 14, 21, and 28 days postsurgery, the hind limb vasculature in the adductor and gastrocnemius muscle regions was imaged using a swept-source optical

coherence tomography (OCT) system as described previously.[36,51] The OCT system has a 100 kHz source with a center wavelength of 1060 nm (Axsun Technologies, Inc.). Speckle variance OCT volumes were acquired noninvasively through the skin in 4 mm × 4 mm areas covering the two muscle regions, and average intensity projections in depth were used to visualize all vessels detected within the imaged volume. After image processing was performed to enhance contrast and enable vessel segmentation,[51,52] morphological parameters including vessel area density (total area filled by vessels/total area of imaged region) and vessel length fraction (total vessel length/total area of imaged region) were quantified.

2.5.7. Post-Traumatic Osteoarthritis Model—For PTOA experiments, 18 C57BL/6 mice (Jackson Laboratory) of equivalent weight (<10% variance) at 10 weeks of age were divided into three different treatment groups: Normal, PBS control, and PPS-MS. The mice in the normal group did not receive any treatment and served as a nonloaded control. Animals in the other two groups received an intra-articular injection of 50 μL of PBS or PPS-MS suspension (2.6 μg/mL) in the left knee joint. The injections were given 24 h prior to exposure to mechanical loading. The PTOA model of noninvasive repetitive joint loading was induced by subjecting the left knee joint of mice (anesthetized with 3% isoflurane) to 40 cycles of compressive mechanical loading at 9 N. This procedure was repeated three times per week over a period of 2 weeks using conditions adapted from previous studies.[53,54] All procedures in this PTOA study were performed according to protocols and experimental procedures approved by the Institutional Animal Care and Use Committee of the University of Tennessee Center for the Health Sciences.

2.5.8. ROS Measurement in Knee Joints in OA Model—The Amplex Red assay was used to confirm the presence of oxidative stress (specifically H_2O_2) in the PTOA model in 6 C57BL/6 mice. Three mice received mechanical loading on both knees, and three mice received no loading. At 14 days after the first joint loading procedure, the knee joint was excised immediately post-mortem, and excess muscle was removed (6 knee joints per group). Tissue was cut from the distal femur and proximal tibia to yield ~200 mg of tissue. Upon excision, knee joints were placed in Kreb's HEPES Buffer (pH 7.35) on ice until assayed (assay began immediately following excision of all knee joints). Amplex Red working solution was prepared as described above (2.5.3). Knee joints were transferred into the Amplex Red solution (500 μL of working solution per well) and incubated in the dark for 1 h at 37 °C. A series of dilutions of H_2O_2 from 15 to 0 μM was prepared in a black-walled 96-well plate at the same time that the tissue incubation began. After 1 h, 150 μL of solution from each sample was transferred to the black 96-well plate, and Amplex Red fluorescence was measured on an IVIS imaging system (Lumina Series III, PerkinElmer) with 530/590 nm excitation/emission filters.

2.5.9. Assessment of Cartilage Damage and Matrix Metalloproteinase (MMP) Activity in PTOA—At the completion of the two-week loading period, mice in the PTOA experimental groups were injected retro-orbitally with a 100 μL composite mixture of 50 μL of monoclonal antibody to type II collagen (MabCII680) labeled with XenoFluor 680 fluorescent dye (XF680; PerkinElmer, Waltham, MA), and 50 μL of 1 nM MMPSense 750

FAST Fluorescent Imaging Agent (MMP750) (PerkinElmer, Waltham, MA), a substrate that fluoresces when enzymatically cleaved by MMPs. After 24 h, the mice were euthanized, skin was removed from the legs, and the knee joints were optically scanned for MabCII and MMP750 fluorescence using a Lumina XR (PerkinElmer, Waltham, MA). MabCII680 detects cartilage damage due to selective binding to exposed CII (which is not accessible in healthy articular surfaces), and MMP750 was used to assess MMP activity in vivo.[55] The fluorescence in each knee joint was quantified using Living Image 4.0 software to calculate the region of interest (ROI) and graphed as radiant efficiency (photons/sec/cm^2/str)/(μW/cm^2).

The imaging results were quantified by selecting the region of interest (ROI) defined as the affected, fluorescent area of the knee compared to the total area of the knee joint. The affected region was measured both in terms of cartilage damage (MabCII680) and MMP activity (MMP750). The results are expressed in terms of average ROI that represents observations obtained from the whole group. This reduced the possibility of sampling bias while selecting the ROI. Previously, we have shown that ROIs measured with this method also correspond to the histological score for OA.[54]

2.5.10. Measurement of Total Nitric Oxide Levels in PTOA—Blood samples were collected from anesthetized mice in the PTOA experiment just prior to euthanasia and clotted at room temperature. They were then centrifuged for 10 min at 1500 rpm, and serum was collected. The sera were stored at −80 °C until analysis for total nitric oxide (NO) levels by directed Griess reaction using a total NO (Nitrate/Nitrite) assay kit (Cayman Chemical, MN).

2.6. Statistical Analysis

All data are reported as mean ± standard error of the mean (SEM). An Analysis of Variance (ANOVA) with a posthoc Tukey test for multiple comparisons was used to determine treatment effects for comparisons between multiple groups (in vitro and in PTOA model). For comparisons between only two groups (HLI model), a Wilcoxon Rank Sum test was used. For longitudinal imaging end points in the HLI model, an ANOVA general linear model (GLM) analysis was performed using the RMS package in R to model the response curves and compare treatment effects at each time point. $p < 0.05$ was considered significant for all analyses.

3. RESULTS

3.1. Microsphere Synthesis and Characterization

3.1.1. Synthesis and Characterization of PPS—PPS was synthesized by anionic polymerization of propylene sulfide as described previously[39] and depicted in Figure 1A. The polymer structure was confirmed by 1H NMR spectra recorded in $CDCl_3$ (Figure 1B): 1.3–1.4 (s, CH_3), 2.5–2.8 (s, −CH), 2.8–3.1 (s, CH_2), 3.72 (t, CH_2−OH). The molecular weight and polydispersity of PPS as determined by GPC were M_n = 6700 g/mol and PDI = 1.1, respectively (Figure 1C).

3.1.2. Microsphere Characterization—PPS-MS were characterized for size and morphology by SEM (Figure 1D and Figure S2). Measurements of microsphere diameters in SEM images resulted in an average diameter of 1.09 ± 0.46 μm (mean ± SD, $n > 600$) and a diameter range of 0.30 to 5.27 μm. Subsequent batches of PPS-MS had average diameters and ranges of 1.10 ± 0.46 μm and 0.2–3.15 μm, 1.13 ± 0.52 μm and 0.18–2.8 μm, and 1.11 ± 0.62 μm and 0.14–4.5 μm, respectively.

3.2. Oxidative Degradation of PPS and ROS-Scavenging in Vitro

3.2.1. PPS Polymer is Oxidized at Different Rates by Various ROS in Vitro—The oxidation of PPS in free polymer form by different ROS was detected using ^{1}H NMR (Figure 2A). ^{1}H NMR of PPS exposed to H_2O_2 (1250 mM) showed a shift in PPS peaks that correlates with oxidized PPS (Figure 2Aii). $^-$OCl (500 mM) completely degraded PPS and no PPS peaks remained in the NMR spectrum (Figure 2Aiii). $ONOO^-$ generated by SIN-1 (50 mM) caused the appearance of oxidized PPS peaks, similar to exposure to H_2O_2, but did not completely oxidize PPS under the conditions tested (Figure 2Aiv). PPS is differentially sensitive to oxidation by these different ROS as determined by ^{1}H NMR analysis (Figure S3). The concentrations that caused 50% oxidation of PPS are 711 mM and 211 mM for H_2O_2 and NaOCl, respectively (Figure S3A, B), and a SIN-1 concentration of 50 mM caused 15% oxidation of PPS relative to baseline (Figure S3C).

GPC was used to detect changes in molecular weight and polydispersity after incubation of the polymer with H_2O_2, $^-$OCl, and $ONOO^-$ (generated by SIN-1). The chromatograms in Figure 2B show shifts in the molecular weight of PPS incubated with these ROS in comparison to a control polymer sample (Figure 2Bi). H_2O_2 (1250 mM) oxidation of PPS caused a shift in the GPC peak (Figure 2Bii). $^-$OCl (500 mM) breaks sulfur–carbon bonds in the PPS, resulting in a disappearance of larger PPS polymer chains visualized by a lack of elution peak at high equivalents of $^-$OCl (Figure 2Biii). However, at lower equivalents of $^-$OCl, there was a decrease in molecular weight and an increase in polydispersity of the polymer chains (data not shown). $ONOO^-$ generated by SIN-1 (50 mM) had little detectable effect on PPS molecular weight as measured by GPC under the conditions tested (Figure 2Biv).

3.2.2. PPS-MS are Degraded by Multiple ROS in Vitro—The degradation of PPS-MS was assessed upon exposure to H_2O_2, $^-$OCl, and $ONOO^-$ (SIN-1) (Figure 2C). Compared to a control microsphere sample (Figure 2Ci), H_2O_2 (1250 mM) and NaOCl (500 mM) caused complete dissolution of the microspheres (Figure 2Cii-iii). $ONOO^-$ generated by SIN-1 (50 mM) also significantly disrupted the microsphere structure, but what appear to be highly swollen microspheres or aggregates of the polymeric byproduct remained visually apparent in the samples (Figure 2Civ). A similar swollen microparticle appearance was observed after incubating PPS-MS with lower concentrations of H_2O_2 (data not shown), suggesting that the lower concentration of SIN-1 affected the microspheres but that oxidation/microsphere degradation was less complete because of the lower $ONOO^-$ dose achievable using commercially available reagents.

3.2.3. PPS-MS Scavenge Hydrogen Peroxide, Peroxynitrite, and Hypochlorite but Not Nitrite or Superoxide in Vitro—The H_2O_2-scavenging activity of PPS-MS was confirmed using Amplex Red. Treatment of a 100 μM H_2O_2 solution with PPS-MS for 1 week significantly reduced Amplex Red fluorescence in a microsphere dose-dependent manner (Figure 3A) (one-way ANOVA, $p < 0.001$). Pyrogallol Red can be used to measure $ONOO^-$, as it is bleached by $ONOO^-$, and this bleaching effect can be reduced or inhibited by antioxidant compounds such as ascorbic acid.[42] In the presence of PPS-MS, PGR was protected from bleaching in a dose-dependent manner with absorbance measured immediately following addition of $ONOO^-$ (Figure 3B, one-way ANOVA $p < 0.0001$). Ascorbic acid was tested as a positive control and resulted in only 2% relative bleaching (nearly complete protection for PGR from $ONOO^-$) (data not shown). The ^-OCl-scavenging activity of PPS-MS was confirmed using a fluorimetric ^-OCl assay. Treatment with PPS-MS significantly reduced ^-OCl levels in vitro after 10 min of incubation (Figure 3C, $p < 0.001$). A nitric oxide assay kit utilizing Griess Reagent was used to determine whether PPS-MS scavenge nitrite (Figure S4A), and the results showed no change in nitrite levels compared to a PBS control. A DHE assay was used to determine whether PPS-MS scavenge O_2^-. The assay results showed no change in DHE fluorescence with PPS-MS treatment in comparison to an untreated O_2^- solution (Figure S4B, C). A decrease in DHE fluorescence was observed with treatment with SOD as a positive control, confirming the veracity of the assay and that O_2^- is not scavenged by PPS-MS. DHE fluorescence was tracked over time to show an increase in O_2^- (produced by the X/XO system) in the no treatment and PPS-MS groups, whereas no increase in DHE fluorescence was detected in the SOD control group (Figure S4C).

3.3. PPS-MS Reduces ROS in LPS-Activated Macrophages in Vitro

3.3.1. PPS-MS Reduce Hydrogen Peroxide Levels in Activated Macrophages—An Amplex Red assay was used to measure extracellular H_2O_2 secreted by RAW cells activated with LPS. Treatment of activated RAW cells with PPS-MS significantly reduced H_2O_2 levels at doses ranging from 100 to 400 μg/mL ($p < 0.001$) relative to activated, untreated cells (Figure 4A). Furthermore, the H_2O_2 levels in PPS-MS-treated cells were statistically equivalent to ROS levels in nonactivated RAW cells ($p > 0.05$).

3.3.2. Measurement of PPS-MS Effects on Multiple Cellular ROS—APF, a derivative of fluorescein that is sensitive to ^-OCl, $OH^{\cdot}$, and $ONOO^-$, was used to measure the effect of PPS-MS on intracellular ROS. PPS-MS doses ranging from 100 to 400 μg/mL significantly reduced APF fluorescent signal compared to the LPS-stimulated, no-treatment control (Figure 4B, $p < 0.001$).

Flow cytometry quantification of general ROS detected by the DCFDA dye confirmed that PPS-MS reduced intracellular ROS levels in activated RAW cells (Figure 4C). DCFDA fluorescence was significantly reduced in activated RAW cells treated with PPS-MS in a dose-dependent manner for doses of 200 to 400 μg/mL ($p < 0.05$). DCFDA reacts with a variety of ROS, including $ONOO^-$ and $OH^{\cdot}$.[45]

3.3.3. PPS-MS are Cytocompatible—PPS-MS treatment retained greater than 80% cell viability at a dose 5 times the maximum dose used for ROS assays (2000 μg/mL compared to 400 μg/mL) (Figure S5). Cell viability using a CellTiter Glo assay showed minimal loss in cell viability with doses of PPS-MS 50–400 μg/mL (Figure S5).

3.4. Diabetic Peripheral Arterial Disease Model Development

To select a model for therapeutic studies with PPS microspheres, we compared the response to ischemic injury for 5 weeks of hyperglycemia in younger mice and 15 weeks of hyperglycemia in an older cohort. Age-matched, nondiabetic mice were included in both the younger (~15 weeks old at time of surgery) and older (~25 weeks old at time of surgery) cohorts. Longitudinal recovery of hemoglobin oxygen saturation (HbSat) in the footpads was measured using hyperspectral imaging. In the younger cohort, the diabetic mice responded to ischemia with an "overshoot" response in comparison to age-matched, nondiabetic mice (at days 14, 21, and 28). This response peaked at day 14 and was followed by regression in the HbSat ratio. In contrast, the older diabetic cohort did not exhibit this overshoot response, and the HbSat ratio slowly recovered, peaking at day 28. The HbSat ratio for the long-term diabetic group was significantly lower than that for the younger mice with 5 weeks of diabetes at days 0 ($p < 0.05$) and 14 ($p < 0.01$) (Figure S6A). In terms of the footpad perfusion ratio measured by LDPI, the younger cohort showed an early overshoot response in the diabetic compared to nondiabetic, age-matched mice. In a manner similar to the HbSat response, this overshoot peaked early in the time course (day 7) and was followed by regression of the LDPI ratio. In the older cohort of mice, the recovery of perfusion was blunted, and the older diabetic mice had significantly lower perfusion than the younger diabetic mice at days 7 ($p < 0.001$) and 14 ($p < 0.01$) (Figure S6B). After observing this impaired functional recovery from ischemia and larger "therapeutic window" in the older, long-term diabetic group, this model of chronic hyperglycemia was selected for evaluating the effects of antioxidant therapy on HLI.

3.5. H_2O_2 is Elevated in Diabetic Mice with Ischemia and in Mechanically Induced PTOA

Elevated ROS was confirmed in the HLI model with prolonged hyperglycemia (15 weeks of diabetes) and in the PTOA model using the Amplex Red assay. Tissue H_2O_2 was measured in freshly excised gastrocnemius muscles in mice with HLI and in excised knee joints with and without OA. In the HLI model, H_2O_2 was elevated in the ischemic gastrocnemius muscle relative to control limbs in both diabetic and nondiabetic mice at day 14 postsurgery (Figure 5A, ischemic/control ratios >1). The relative H_2O_2 level was significantly greater in the muscle of diabetic mice than that of nondiabetic mice ($p < 0.05$). In the PTOA model, H_2O_2 was significantly increased in injured knees after 2 weeks of loading compared to control knees (Figure 5B).

3.6. PPS-MS Treatment of Hind Limb Ischemia in Long-Term Hyperglycemic Mice

3.6.1. PPS-MS Treatment Improves Distal (footpad) Response to HLI—Hemoglobin oxygen saturation was measured in the footpads of diabetic mice treated with saline or PPS-MS at the time of hind limb ischemia surgery (Figure 6A). A *t*-test performed on the GLM of the longitudinal response curves showed that the PPS-MS and saline-treated

groups differed significantly from days 19 to 28 ($p < 0.05$) (Figure 6A, raw data in Figure S7A). The perfusion ratio was also measured to assess the effect of microsphere treatment on the response to ischemia (Figure 6B). At day 14, the perfusion ratio for the PPS-MS group was significantly greater than that of the saline group ($p < 0.05$) (Figure S7B). Similarly, a *t* test performed on the longitudinal response curves generated by the GLM analysis confirms that perfusion ratios were significantly higher for the microsphere-treated group compared to the saline group for the latter half of the time course ($p < 0.05$, days 19–28) (Figure 6B).

3.6.2. Noninvasive Imaging of Hind Limb Vascular Morphology Changes in Response to Therapy—Speckle variance OCT[51,52] was used to image the longitudinal vascular response to PPS-MS therapy in the ischemic adductor and gastrocnemius muscle regions (Figure 6C–F). Representative time course images from one animal in each treatment group are shown for the adductor and gastrocnemius regions in Figure S8, and images for four animals from each group are provided for day 7 in Figure S9. Qualitatively, vascular morphology in the adductor looked similar among the treatment groups at the start and end of the time course, with an apparent increase in vessel density in the microsphere-treated group relative to the saline group at intermediate time points such as day 7 (Figure S9), suggesting that PPS-MS treatment accelerated recovery to a consistent steady state. In the gastrocnemius muscle, there was greater variability in vessel density at early and intermediate time points compared to the end of the time course, and vascular remodeling was lagging in the saline group (Figures S8 and S9).

In the adductor muscle, vessel area density (Figure S10A) and vessel length fraction (Figure S10C) were significantly greater in microsphere-treated group at day 7 ($p < 0.01$). GLM analysis of the longitudinal response in the adductor also revealed significant increases in vessel area density (Figure 6C) and vessel length fraction (Figure S10E) in the PPS-MS group relative to the saline group during the second and third weeks postsurgery.

In the gastrocnemius muscle, vessel area density was significantly lower in the saline-treated group from day 0 through day 14 relative to the PPS-MS group ($p < 0.05$) (Figure S10B). Similarly, vessel length fraction in the gastrocnemius muscle was significantly lower in the saline group for days 0 through 7 ($p < 0.05$) (Figure S10D). GLM analysis of the longitudinal response in the gastrocnemius also indicated that there were significant differences in vessel area density (Figure 6D) and vessel length fraction (Figure S10F) between the treatment groups over similar ranges in time.

3.6.3. PPS-MS Treatment Reduces Cartilage Damage and MMP Activity in PTOA—IVIS imaging was used to analyze the effects of PPS-MS treatment on the PTOA mouse model as the fluorescence signal for MabCII680 and MMP750 correspond directly to cartilage damage and MMP activity, respectively (Figure 7A). MMPSense is an MMP cleavable probe that uses a quenched fluorophore that emits fluorescence after cleavage. MabCII is a collagen II-specific, fluorescently tagged antibody that preferentially binds to exposed collagen II on damaged articular cartilage. No fluorescence signal was observed for the normal animals without mechanical loading (Figure 7A). However, intense fluorescence signal from both reporters was observed for mice that received mechanical loading and

treatment with PBS. Significant decreases in fluorescence signal from MabCII680 (Figure 7B) and MMP750 (Figure 7C) were observed for the mechanically loaded mice treated with PPS-MS ($p < 0.05$). These results suggest treatment of mice with PPS-MS attenuated the cartilage damage and MMP activity as compared with the group treated with PBS alone.

3.6.4. Systemic Nitric Oxide Levels Are Reduced with PPS-MS Treatment in PTOA Model—Mechanical stress is well-known to play a part in the pathogenesis of OA by inducing oxidative stress.[56] In previous studies, higher concentrations of total NO (nitrites and nitrates) have been found in the blood of patients with arthritis.[57] Therefore, the oxidative stress was measured by examining the total NO level in serum in all three groups (Figure 7D). It is evident that PPS-MS treatment significantly attenuated the oxidative stress after mechanical loading when compared to the PBS-treated group ($p < 0.05$).

4. DISCUSSION

Transient or low levels of ROS contribute to cell signaling that promotes both homeostasis under normal conditions and repair following injury. However, chronic or high levels of ROS can be detrimental to vascular function[15,58,59] and preservation of tissue such as articular cartilage following injury.[19,60] Therefore, we explored the therapeutic effects of a local depot of antioxidant PPS-based microspheres in models of diabetic PAD and PTOA. In these disease models, oxidative stress is present for at least 2 weeks (Figure 5), and sustained therapy without repeated injections would be beneficial. PPS was selected as the polymer for the microspheres because it scavenges H_2O_2 (Figure 3A), $ONOO^-$ (Figure 3B), and ^-OCl (Figure 3C), protects cells from H_2O_2-induced toxicity,[36,39] and can be used to deliver hydrophobic therapeutic molecules via ROS-responsive drug release.[36] PPS-MS treatment also reduces extracellular H_2O_2 (Figure 4A) and intracellular ^-OCl, $OH^{\cdot}$, and $ONOO^-$ (Figure 4B, C) in LPS-stimulated macrophages. The concept of targeting multiple ROS has been previously demonstrated in vitro in a hybrid polymer–enzyme nanocarrier system.[33] However, micron-sized particles are large enough to form a stable depot that is retained in the tissue interstitium without significant diffusion away from the injection site. In previous work, we have demonstrated that PPS-MS remain as a localized depot in ischemic and healthy hind limb muscle tissue for a minimum of 21 days.[36] Others have shown that 1 μm sized particles have greater retention than smaller, nanosized particles in the intra-articular space of the knee joint, remaining detectable in the joint for greater than 14 days.[61] Furthermore, targeting a particle size of approximately 1 μm enables preferential uptake by phagocytic immune cells, targeting the antioxidant effect to the relevant inflammation-associated cells.[36] Therefore, fabrication of particles in this size range was targeted in order to achieve a combination of both intracellular and extracellular ROS scavenging, which is important for optimal cell and tissue protection from oxidative stress.[62] Additionally, as we have previously established, PPS-MS can be extended to achieve locally sustained drug release.[36]

In the context of vascular disease models, the inhibition of ROS in healthy animals has shown that ROS are key players in angiogenesis during normal recovery.[15,63,64] This effect is believed to be due to the roles of H_2O_2 in stimulating migration and proliferation in endothelial cells[63,64] and the role of NADPH oxidase-derived ROS in modulating VEGF-A

expression and vascular smooth muscle cell proliferation.[15] In fact, infusion of the H_2O_2 and $ONOO^-$ scavenger ebselen reduces perfusion recovery and capillary density,[63] and otherwise healthy mice lacking the $gp91^{phox}$ (Nox2) subunit of NADPH oxidase have impaired neovascularization.[15,59,63] However, studies using preclinical models of chronic oxidative stress (i.e., aged, diabetic animals) have demonstrated the potential for antioxidant treatment to improve neovascularization and vascular function in these situations that better reflect aged human pathology.[13,15,24,65,66] Diabetes is a known risk factor for atherosclerosis and is associated with increased prevalence of PAD,[67] so the development of more effective treatments for mitigating vascular dysfunction is of significant interest. Scavenging ROS with superoxide dismutase and/or catalase mimetics is a promising approach, but to date these treatments have generally been administered systemically in preclinical models.[13,24,68] In contrast, PPS microspheres[36] administered as a localized ROS-scavenging therapeutic treatment offer the opportunity to avoid off-target effects in tissues with physiologically appropriate levels of ROS.[58]

Prior to evaluating the effect of the PPS-MS on recovery from HLI, we compared the response to HLI in younger mice with 5 weeks of presurgical hyperglycemia to older mice with 15 weeks of hyperglycemia prior to surgery. The duration of hyperglycemia prior to experimental manipulation varies among previously reported studies of the vascular response to ischemia;[13,15,65,66,69] however, the effects of diabetes on vascular function have been shown to be disease-duration-dependent.[70–72] Susceptibility to STZ and the severity of the resulting hyperglycemia and other symptoms varies with mouse strain,[73] so we used FVB mice, which are susceptible to robust, persistent hyperglycemia after a low dose STZ protocol and have demonstrated improved neovascularization with antioxidant and anti-inflammatory therapies.[65,66] After induction of HLI, an "overshoot" response was observed in footpad hemoglobin saturation and perfusion ratios in the younger diabetic group, but not in the age-matched nondiabetic group or the older groups (Figure S6). The overshoot response followed by regression is similar to that observed in diabetic C57BL6/J mice which had more pronounced vessel growth and vessel rarefaction phases in comparison to nondiabetic controls.[69] In contrast, the older cohort of mice in the current study showed a slower rate of recovery from ischemia. Additionally, the mice with 15 weeks of diabetes showed significant oxidative stress in the ischemic gastrocnemius muscle (Figure 5A). Taken together, these results indicate that the mice in the older cohort with 15 weeks of diabetes have a significant "therapeutic window" for reducing oxidative stress in the muscle and improving the vascular response to HLI at early time points. Therefore, this model of diabetic PAD was selected to evaluate the therapeutic effect of PPS-MS.

The functional effects of PPS-MS were evaluated in the diabetic HLI model using perfusion, hemoglobin oxygen saturation, and vessel morphology as end points. PPS-MS were injected at the time of injury, because ROS levels increase rapidly in this model of PAD (elevated ROS in the muscle by day 1 postsurgery).[36] Although some amount of ROS is beneficial to angiogenesis[15] and too much ROS scavenging could be detrimental,[59,63] the antioxidant PPS-MS improved functional recovery from HLI in our long-term diabetic model. In mice treated with PPS-MS, there were significant increases in HbSat and perfusion in the footpads (Figure 6A, B and Figure S7) as well as earlier vessel remodeling in the adductor and gastrocnemius (Figure 6C–F, Figure S8–S10) in comparison to saline-treated mice.

Observation of these functional benefits suggest that PPS-MS are promising for targeting local oxidative stress and improving the vascular response to ischemia in mice with prolonged hyperglycemia.

Similarly, PPS-MS have promise for localized oxidative stress reduction in PTOA. OA is a complex disease process that occurs over a long period of time, but it begins with early focal, superficial lesions in the articular cartilage followed by the loss of proteoglycans and breakdown of cartilage collagen. Type II collagen is present in meniscal and articular cartilages but is inaccessible to antibodies in the normal, healthy joint. IVIS imaging of the binding of type II collagen antibody in the mechanically loaded knee confirms that significant degradation of knee joint cartilage occurs in the context of mechanical loading, leading to the unmasking of the type II collagen (Figure 7A, B). This is in agreement with our previous observations that MabCII680 binding correlates with the histological score for OA.[54] The presence of active MMP levels in the joint is suggestive that the MMP enzymes secreted by the synovium or the chondrocytes themselves might play a role in this unmasking. A member of the MMP family, MMP-13 (collagenase-3), is the primary enzyme responsible for the degradation of type II collagen in the cartilage matrix in osteoarthritic cartilage.[74]

The ROS generated in response to mechanical injury regulate expression of numerous genes involved in immune and inflammatory responses including MMP-13.[60] Our results showed that mechanical loading causes cartilage destruction, increased MMP activity (Figure 7A–C), and oxidative stress (Figure 5B). Furthermore, systemic NO levels increased significantly after repeated mechanical loading cycles (Figure 7D). Previous studies have implicated oxidative stress in the pathogenesis and progression of OA.[19] In the current work, we show that treatment of knee joints with an intra-articular injection of PPS-MS significantly attenuated cartilage damage and MMP activity in the PTOA model (Figure 7). In this proof-of-concept preclinical study, PPS-MS were injected 1 day prior to initiation of mechanical loading injury, and the results of this study suggest that targeting early oxidative stress in PTOA with a local depot of chondroprotective PPS-MS can attenuate further cartilage degradation by decreasing MMP activity and total NO production. Impeding OA at its early stages is crucial in building an effective therapeutic regime against OA,[75] so clinical translation of an antioxidant therapy such as PPS-MS would ideally consist of intervention as soon as possible following joint injury.

5. CONCLUSIONS

There is a significant need for long-lasting and well-controlled therapies for inflammatory diseases such as diabetic PAD and PTOA. Two decades of clinical trials have yielded inconsistent outcomes and no new Food and Drug Administration-approved therapies for PAD.[76] Additionally, there are currently no pharmacological treatments for OA that treat the underlying molecular cause of disease.[77] In this work, oxidation-sensitive PPS was used to formulate microspheres for local antioxidant therapy. The microspheres are capable of scavenging multiple ROS including H_2O_2, ^{-}OCl, and $ONOO^{-}$, which are implicated in disease progression. In vivo studies demonstrated that PPS-MS provide improvements in multiple functional measures of vascular recovery in a diabetic PAD model as well as

impede progression of cartilage damage in a PTOA model. These collective results suggest that targeting ROS in these models is an effective therapeutic strategy. In sum, the results establish PPS-MS as a promising stand-alone therapy or as a drug delivery vehicle that may synergize with PTOA and diabetic PAD therapeutics.

Supplementary Material

Refer to Web version on PubMed Central for supplementary material.

Acknowledgments

The authors thank Fang Yu, John Martin, Melissa Markham, Dan Gil, and Mary Dockery for assistance with experiments, and Jeffrey M. Davidson for use of the LDPI.

Funding

This work was supported by a Vanderbilt Discovery Grant, NIH R21 HL109748; American Heart Association Grant-in-Aid 12GRNT 12060235; and DOD PRORP OR130302. K.P.O. was supported by a P.E.O. Scholar Award and an NSF Graduate Research Fellowship DGE-0909667. T.E.K was supported by the NSF Graduate Research Fellowship Program under Grant 1445197. K.A.H and H.C. were supported by funds from a VA Merit Award.

References

1. D'Autreaux B, Toledano MB. ROS as signalling molecules: mechanisms that generate specificity in ROS homeostasis. Nat Rev Mol Cell Biol. 2007; 8:813–824. [PubMed: 17848967]
2. Finkel T, Holbrook NJ. Oxidants, oxidative stress and the biology of ageing. Nature. 2000; 408:239–247. [PubMed: 11089981]
3. Dziubla T, Butterfield DA. Oxidative Stress and Biomaterials. Academic Press; Cambridge, U.K.: 2016.
4. Siwik DA, Pagano PJ, Colucci WS. Oxidative Stress Regulates Collagen Synthesis and Matrix Metalloproteinase Activity in Cardiac Fibroblasts. Am J Physiol Cell Physiol. 2001; 280:C53–C60. [PubMed: 11121376]
5. Henrotin Y, Kurz B, Aigner T. Oxygen and reactive oxygen species in cartilage degradation: friends or foes? Osteoarthritis and cartilage. 2005; 13:643–654. [PubMed: 15936958]
6. Ziskoven C, Jäger M, Zilkens C, Bloch W, Brixius K, Krauspe R. Oxidative stress in secondary osteoarthritis: from cartilage destruction to clinical presentation? Orthop Rev. 2010; 2:23.
7. Giugliano D, Ceriello A, Paolisso G. Oxidative stress and diabetic vascular complications. Diabetes Care. 1996; 19:257–267. [PubMed: 8742574]
8. Brownlee M. Biochemistry and molecular cell biology of diabetic complications. Nature. 2001; 414:813–820. [PubMed: 11742414]
9. American Diabetes Association. Peripheral arterial disease in people with diabetes. Diabetes Care. 2003; 26:3333–3341. [PubMed: 14633825]
10. Ruiter MS, van Golde JM, Schaper NC, Stehouwer CD, Huijberts MS. Diabetes impairs arteriogenesis in the peripheral circulation: review of molecular mechanisms. Clin Sci. 2010; 119:225–238. [PubMed: 20545627]
11. Case J, Ingram DA, Haneline LS. Oxidative stress impairs endothelial progenitor cell function. Antioxid Redox Signaling. 2008; 10:1895–1907.
12. Woo CH, Shishido T, McClain C, Lim JH, Li JD, Yang J, Yan C, Abe J. Extracellular signal-regulated kinase 5 SUMOylation antagonizes shear stress-induced antiinflammatory response and endothelial nitric oxide synthase expression in endothelial cells. Circ Res. 2008; 102:538–545. [PubMed: 18218985]
13. Ceradini DJ, Yao D, Grogan RH, Callaghan MJ, Edelstein D, Brownlee M, Gurtner GC. Decreasing intracellular superoxide corrects defective ischemia-induced new vessel formation in diabetic mice. J Biol Chem. 2008; 283:10930–10938. [PubMed: 18227068]

14. Forstermann U. Nitric oxide and oxidative stress in vascular disease. Pfluegers Arch. 2010; 459:923–939. [PubMed: 20306272]
15. Ebrahimian TG, Heymes C, You D, Blanc-Brude O, Mees B, Waeckel L, Duriez M, Vilar J, Brandes RP, Levy BI, Shah AM, Silvestre JS. NADPH oxidase-derived overproduction of reactive oxygen species impairs postischemic neovascularization in mice with type 1 diabetes. Am J Pathol. 2006; 169:719–728. [PubMed: 16877369]
16. Cai H, Harrison DG. Endothelial dysfunction in cardiovascular diseases: the role of oxidant stress. Circ Res. 2000; 87:840–844. [PubMed: 11073878]
17. Halliwell B. Free radicals and other reactive species in disease. eLS. 2005; doi: 10.1038/npg.els.0003913
18. Sarban S, Kocyigit A, Yazar M, Isikan UE. Plasma total antioxidant capacity, lipid peroxidation, and erythrocyte antioxidant enzyme activities in patients with rheumatoid arthritis and osteoarthritis. Clin Biochem. 2005; 38:981–986. [PubMed: 16150434]
19. Henrotin YE, Bruckner P, Pujol JP. The role of reactive oxygen species in homeostasis and degradation of cartilage. Osteoarthritis and cartilage. 2003; 11:747–755. [PubMed: 13129694]
20. Afonso V, Champy R, Mitrovic D, Collin P, Lomri A. Reactive oxygen species and superoxide dismutases: role in joint diseases. Jt, Bone, Spine. 2007; 74:324–329.
21. Loeser RF. Molecular mechanisms of cartilage destruction in osteoarthritis. J Musculoskelet Neuronal Interact. 2008; 8:303–306. [PubMed: 19147949]
22. Collins JA, Wood ST, Nelson KJ, Rowe MA, Carlson CS, Chubinskaya S, Poole LB, Furdui CM, Loeser RF. Oxidative Stress Promotes Peroxiredoxin Hyperoxidation and Attenuates Pro-survival Signaling in Aging Chondrocytes. J Biol Chem. 2016; 291:6641–6654. [PubMed: 26797130]
23. Kim HW, Lin A, Guldberg RE, Ushio-Fukai M, Fukai T. Essential role of extracellular SOD in reparative neovascularization induced by hindlimb ischemia. Circ Res. 2007; 101:409–419. [PubMed: 17601801]
24. Nassar T, Kadery B, Lotan C, Da'as N, Kleinman Y, Haj-Yehia A. Effects of the superoxide dismutase-mimetic compound tempol on endothelial dysfunction in streptozotocin-induced diabetic rats. Eur J Pharmacol. 2002; 436:111–118. [PubMed: 11834254]
25. Thiemermann C. Membrane-permeable radical scavengers (tempol) for shock, ischemia-reperfusion injury, and inflammation. Crit Care Med. 2003; 31:S76–84. [PubMed: 12544980]
26. Pua ML, Yoshitomi T, Chonpathompikunlert P, Hirayama A, Nagasaki Y. Redox-active injectable gel using thermo-responsive nanoscale polyion complex flower micelle for noninvasive treatment of local inflammation. J Controlled Release. 2013; 172:914–920.
27. Monti E, Supino R, Colleoni M, Costa B, Ravizza R, Gariboldi MB. Nitroxide TEMPOL impairs mitochondrial function and induces apoptosis in HL60 cells. J Cell Biochem. 2001; 82:271–276. [PubMed: 11527152]
28. Hood ED, Chorny M, Greineder CF, S Alferiev I, Levy RJ, Muzykantov VR. Endothelial targeting of nanocarriers loaded with antioxidant enzymes for protection against vascular oxidative stress and inflammation. Biomaterials. 2014; 35:3708–3715. [PubMed: 24480537]
29. Reddy MK, Labhasetwar V. Nanoparticle-mediated delivery of superoxide dismutase to the brain: an effective strategy to reduce ischemia-reperfusion injury. FASEB J. 2009; 23:1384–1395. [PubMed: 19124559]
30. Yun X, Maximov VD, Yu J, Zhu H, Vertegel AA, Kindy MS. Nanoparticles for targeted delivery of antioxidant enzymes to the brain after cerebral ischemia and reperfusion injury. J Cereb Blood Flow Metab. 2013; 33:583–592. [PubMed: 23385198]
31. Fiore VF, Lofton MC, Roser-Page S, Yang SC, Roman J, Murthy N, Barker TH. Polyketal microparticles for therapeutic delivery to the lung. Biomaterials. 2010; 31:810–817. [PubMed: 19846216]
32. Giovagnoli S, Luca G, Casaburi I, Blasi P, Macchiarulo G, Ricci M, Calvitti M, Basta G, Calafiore R, Rossi C. Long-term delivery of superoxide dismutase and catalase entrapped in poly-(lactide-co-glycolide) microspheres: in vitro effects on isolated neonatal porcine pancreatic cell clusters. J Controlled Release. 2005; 107:65–77.
33. Hu P, Tirelli N. Scavenging ROS: superoxide dismutase/catalase mimetics by the use of an oxidation-sensitive nanocarrier/enzyme conjugate. Bioconjugate Chem. 2012; 23:438–449.

34. Yoshitomi T, Hirayama A, Nagasaki Y. The ROS scavenging and renal protective effects of pH-responsive nitroxide radical-containing nanoparticles. Biomaterials. 2011; 32:8021–8028. [PubMed: 21816462]
35. Tang H, Cao W, Kasturi SP, Ravindran R, Nakaya HI, Kundu K, Murthy N, Kepler TB, Malissen B, Pulendran B. The T helper type 2 response to cysteine proteases requires dendritic cell-basophil cooperation via ROS-mediated signaling. Nat Immunol. 2010; 11:608–617. [PubMed: 20495560]
36. Poole KM, Nelson CE, Joshi RV, Martin JR, Gupta MK, Haws SC, Kavanaugh TE, Skala MC, Duvall CL. ROS-responsive microspheres for on demand antioxidant therapy in a model of diabetic peripheral arterial disease. Biomaterials. 2015; 41:166–175. [PubMed: 25522975]
37. Napoli A, Valentini M, Tirelli N, Muller M, Hubbell JA. Oxidation-responsive polymeric vesicles. Nat Mater. 2004; 3:183–189. [PubMed: 14991021]
38. Gupta MK, Meyer TA, Nelson CE, Duvall CL. Poly(PS-b-DMA) micelles for reactive oxygen species triggered drug release. J Controlled Release. 2012; 162:591–598.
39. Gupta MK, Martin JR, Werfel TA, Shen T, Page JM, Duvall CL. Cell Protective, ABC Triblock Polymer-Based Thermoresponsive Hydrogels with ROS-Triggered Degradation and Drug Release. J Am Chem Soc. 2014; 136:14896–14902. [PubMed: 25254509]
40. Shahani K, Swaminathan SK, Freeman D, Blum A, Ma L, Panyam J. Injectable sustained release microparticles of curcumin: a new concept for cancer chemoprevention. Cancer Res. 2010; 70:4443–4452. [PubMed: 20460537]
41. Jeffery H, Davis SS, O'Hagan DT. The Preparation and Characterization of Poly(Lactide-Co-Glycolide) Microparticles 0.1. Oil-in-Water Emulsion Solvent Evaporation. Int J Pharm. 1991; 77:169–175.
42. Balavoine GG, Geletii YV. Peroxynitrite scavenging by different antioxidants. Part I: convenient assay. Nitric Oxide. 1999; 3:40–54. [PubMed: 10355895]
43. Zhao H, Kalivendi S, Zhang H, Joseph J, Nithipatikom K, Vasquez-Vivar J, Kalyanaraman B. Superoxide reacts with hydroethidine but forms a fluorescent product that is distinctly different from ethidium: potential implications in intracellular fluorescence detection of superoxide. Free Radical Biol Med. 2003; 34:1359–1368. [PubMed: 12757846]
44. Nazarewicz RR, Bikineyeva A, Dikalov SI. Rapid and specific measurements of superoxide using fluorescence spectroscopy. J Biomol Screening. 2013; 18:498–503.
45. Setsukinai K-iUrano Y, Kakinuma K, Majima HJ, Nagano T. Development of novel fluorescence probes that can reliably detect reactive oxygen species and distinguish specific species. J Biol Chem. 2003; 278:3170–3175. [PubMed: 12419811]
46. Like AA, Rossini AA. Streptozotocin-induced pancreatic insulitis: new model of diabetes mellitus. Science. 1976; 193:415–417. [PubMed: 180605]
47. Couffinhal T, Silver M, Zheng LP, Kearney M, Witzenbichler B, Isner JM. Mouse model of angiogenesis. Am J Pathol. 1998; 152:1667–1679. [PubMed: 9626071]
48. Poole KM, Tucker-Schwartz JM, Sit WW, Walsh AJ, Duvall CL, Skala MC. Quantitative optical imaging of vascular response in vivo in a model of peripheral arterial disease. American journal of physiology Heart and circulatory physiology. 2013; 305:H1168–1180. [PubMed: 23955718]
49. Palmer GM, Fontanella AN, Shan S, Hanna G, Zhang G, Fraser CL, Dewhirst MW. In vivo optical molecular imaging and analysis in mice using dorsal window chamber models applied to hypoxia, vasculature and fluorescent reporters. Nat Protoc. 2011; 6:1355–1366. [PubMed: 21886101]
50. Sorg BS, Moeller BJ, Donovan O, Cao Y, Dewhirst MW. Hyperspectral imaging of hemoglobin saturation in tumor microvasculature and tumor hypoxia development. J Biomed Opt. 2005; 10:044004.
51. Poole KM, McCormack DR, Patil CA, Duvall CL, Skala MC. Quantifying the vascular response to ischemia with speckle variance optical coherence tomography. Biomed Opt Express. 2014; 5:4118. [PubMed: 25574425]
52. Poole KM, Patil CA, Nelson CE, McCormack DR, Madonna MC, Duvall CL, Skala MC. Longitudinal study of arteriogenesis with swept source optical coherence tomography and hyperspectral imaging. Proceedings of SPIE, Optical Coherence Tomography and Coherence Domain Optical Methods in Biomedicine XVIII; San Francisco, CA. Feb 1, 2014; Bellingham, WA: SPIE; 2014.

53. Poulet B, Hamilton RW, Shefelbine S, Pitsillides AA. Characterizing a novel and adjustable noninvasive murine joint loading model. Arthritis Rheum. 2011; 63:137–147. [PubMed: 20882669]
54. Cho H, Pinkhassik E, David V, Stuart JM, Hasty KA. Detection of early cartilage damage using targeted nanosomes in a post-traumatic osteoarthritis mouse model. Nanomedicine. 2015; 11:939–946. [PubMed: 25680539]
55. Cho H, Bhatti FUR, Lee S, Brand DD, Yi AK, Hasty KA. In vivo dual fluorescence imaging to detect joint destruction. Artif Organs. 2016; 40:1009. [PubMed: 27183538]
56. Buckwalter JA, Anderson DD, Brown TD, Tochigi Y, Martin JA. The Roles of Mechanical Stresses in the Pathogenesis of Osteoarthritis: Implications for Treatment of Joint Injuries. Cartilage. 2013; 4:286–294. [PubMed: 25067995]
57. Farrell AJ, Blake DR, Palmer R, Moncada S. Increased concentrations of nitrite in synovial fluid and serum samples suggest increased nitric oxide synthesis in rheumatic diseases. Ann Rheum Dis. 1992; 51:1219–1222. [PubMed: 1466599]
58. Kim YW, Byzova TV. Oxidative stress in angiogenesis and vascular disease. Blood. 2014; 123:625–631. [PubMed: 24300855]
59. Urao N, Inomata H, Razvi M, Kim HW, Wary K, McKinney R, Fukai T, Ushio-Fukai M. Role of nox2-based NADPH oxidase in bone marrow and progenitor cell function involved in neovascularization induced by hindlimb ischemia. Circ Res. 2008; 103:212–220. [PubMed: 18583711]
60. Ziskoven C, Jager M, Zilkens C, Bloch W, Brixius K, Krauspe R. Oxidative stress in secondary osteoarthritis: from cartilage destruction to clinical presentation? Orthop Rev. 2010; 2:23.
61. Singh A, Agarwal R, Diaz-Ruiz CA, Willett NJ, Wang P, Lee LA, Wang Q, Guldberg RE, García AJ. Nanoengineered Particles for Enhanced Intra-Articular Retention and Delivery of Proteins. Adv Healthcare Mater. 2014; 3:1562–1567.
62. Shuvaev VV, Muzykantov VR. Targeted modulation of reactive oxygen species in the vascular endothelium. J Controlled Release. 2011; 153:56–63.
63. Tojo T, Ushio-Fukai M, Yamaoka-Tojo M, Ikeda S, Patrushev N, Alexander RW. Role of gp91(phox) (Nox2)-containing NAD(P)H oxidase in angiogenesis in response to hindlimb ischemia. Circulation. 2005; 111:2347–2355. [PubMed: 15867174]
64. Hodara R, Weiss D, Joseph G, Velasquez-Castano JC, Landazuri N, Han JW, Yoon YS, Taylor WR. Overexpression of catalase in myeloid cells causes impaired postischemic neovascularization. Arterioscler, Thromb, Vasc Biol. 2011; 31:2203–2209. [PubMed: 21799178]
65. Huang PH, Tsai HY, Wang CH, Chen YH, Chen JS, Lin FY, Lin CP, Wu TC, Sata M, Chen JW, Lin SJ. Moderate intake of red wine improves ischemia-induced neovascularization in diabetic mice–roles of endothelial progenitor cells and nitric oxide. Atherosclerosis. 2010; 212:426–435. [PubMed: 20637466]
66. Huang PH, Lin CP, Wang CH, Chiang CH, Tsai HY, Chen JS, Lin FY, Leu HB, Wu TC, Chen JW, Lin SJ. Niacin improves ischemia-induced neovascularization in diabetic mice by enhancement of endothelial progenitor cell functions independent of changes in plasma lipids. Angiogenesis. 2012; 15:377–389. [PubMed: 22467057]
67. Marso SP, Hiatt WR. Peripheral arterial disease in patients with diabetes. J Am Coll Cardiol. 2006; 47:921–929. [PubMed: 16516072]
68. Banday AA, Marwaha A, Tallam LS, Lokhandwala MF. Tempol reduces oxidative stress, improves insulin sensitivity, decreases renal dopamine D1 receptor hyperphosphorylation, and restores D1 receptor-G-protein coupling and function in obese Zucker rats. Diabetes. 2005; 54:2219–2226. [PubMed: 15983225]
69. Landazuri N, Joseph G, Guldberg RE, Taylor WR. Growth and regression of vasculature in healthy and diabetic mice after hindlimb ischemia. Am J Physiol Regul Integr Comp Physiol. 2012; 303:R48–56. [PubMed: 22573106]
70. Pieper GM. Enhanced, unaltered and impaired nitric oxide-mediated endothelium-dependent relaxation in experimental diabetes mellitus: importance of disease duration. Diabetologia. 1999; 42:204–213. [PubMed: 10064101]

71. Perreault M, Dombrowski L, Marette A. Mechanism of impaired nitric oxide synthase activity in skeletal muscle of streptozotocin-induced diabetic rats. Diabetologia. 2000; 43:427–437. [PubMed: 10819235]

72. Nagareddy PR, Xia Z, McNeill JH, MacLeod KM. Increased expression of iNOS is associated with endothelial dysfunction and impaired pressor responsiveness in streptozotocin-induced diabetes. Am J Physiol Heart Circulatory Phys. 2005; 289:H2144–2152.

73. Qi Z, Fujita H, Jin J, Davis LS, Wang Y, Fogo AB, Breyer MD. Characterization of susceptibility of inbred mouse strains to diabetic nephropathy. Diabetes. 2005; 54:2628–2637. [PubMed: 16123351]

74. Little CB, Barai A, Burkhardt D, Smith SM, Fosang AJ, Werb Z, Shah M, Thompson EW. Matrix metalloproteinase 13-deficient mice are resistant to osteoarthritic cartilage erosion but not chondrocyte hypertrophy or osteophyte development. Arthritis Rheum. 2009; 60:3723–3733. [PubMed: 19950295]

75. Chu CR, Williams AA, Coyle CH, Bowers ME. Early diagnosis to enable early treatment of pre-osteoarthritis. Arthritis Res Ther. 2012; 14:212. [PubMed: 22682469]

76. Cooke JP, Losordo DW. Modulating the vascular response to limb ischemia: angiogenic and cell therapies. Circ Res. 2015; 116:1561–1578. [PubMed: 25908729]

77. Kavanaugh TE, Werfel TA, Cho H, Hasty KA, Duvall CL. Particle-based technologies for osteoarthritis detection and therapy. Drug Delivery Transl Res. 2016; 6:132–147.

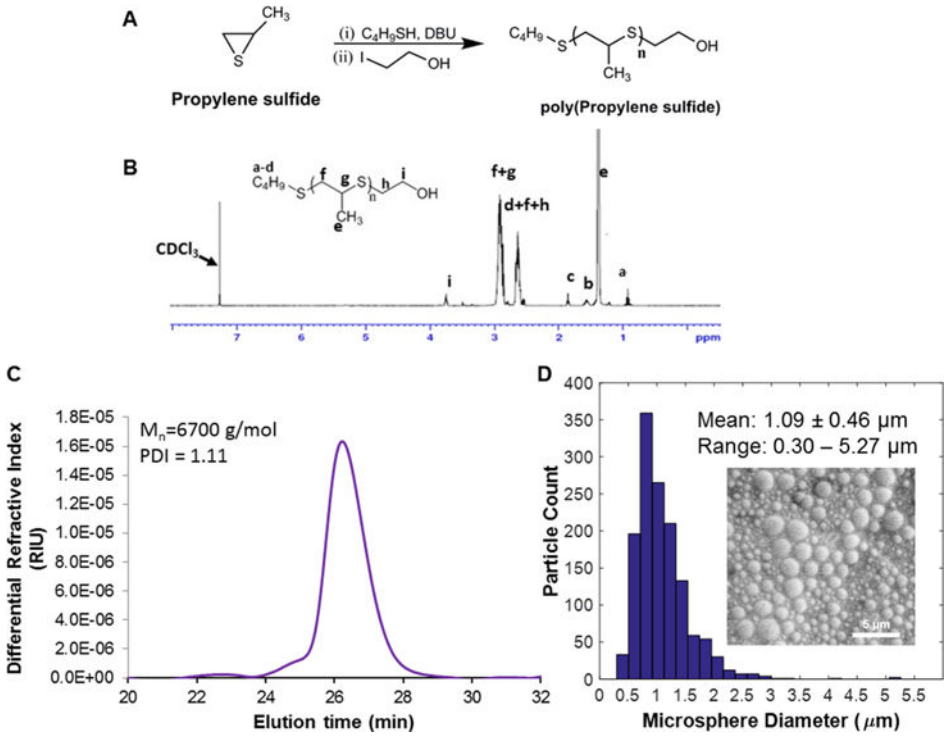

Figure 1.

Characterization of the PPS polymer and microspheres. (A) Synthesis of poly(propylene sulfide) by anionic polymerization. (B) ^{1}H NMR spectrum for PPS polymer. (C) Average molecular weight (M_n = 6700 g/mol) and polydispersity (PDI = 1.1) of the PPS were assessed by GPC. (D) The size distribution of the PPS-MS was measured with SEM, and the mean diameter and diameter range were 1.09 ± 0.46 μm and 0.30–5.27 μm, respectively.

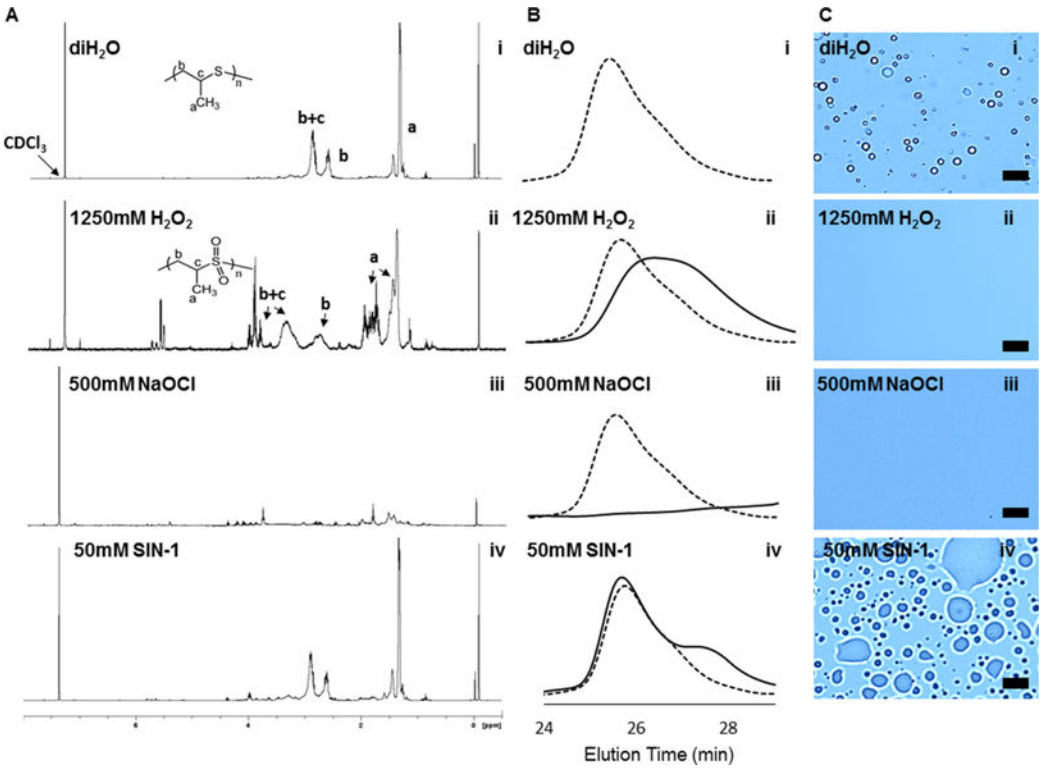

Figure 2.

Oxidation of PPS in the presence of various ROS species. (A) ^{1}H NMR of PPS after 24 h of exposure to different types of ROS media. (B) GPC traces of PPS polymer (dotted trace) and oxidized PPS polymer (solid trace) 24 h after ROS exposure. (C) Visualized degradation of PPS-MS in the presence of H_2O_2, $^{-}$OCl (NaOCl), and $ONOO^{-}$ (SIN-1) at 24 h after exposure to ROS. Scale bar = 10 μm. For columns A–C, row (i) represents PBS control, (ii) is treatment with H_2O_2, (iii) is treatment with $^{-}$OCl, and (iv) is treatment with $ONOO^{-}$ (SIN-1).

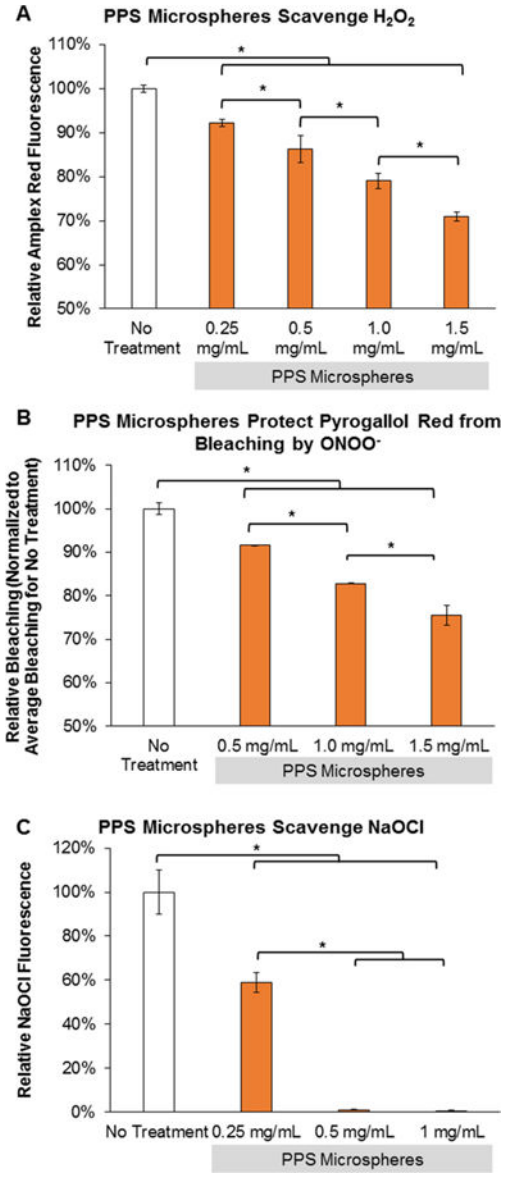

Figure 3.

PPS-MS exhibit antioxidant properties for multiple types of ROS. (A) PPS-MS significantly reduce Amplex Red fluorescence in a microsphere dose-dependent manner following 1 week of incubation with 100 μM H_2O_2 (one-way ANOVA, $p < 0.001$, *significant posthoc comparisons). (B) PPS-MS protect PGR from bleaching by $ONOO^-$ in a dose-dependent manner (one-way ANOVA $p < 0.0001$, *significant posthoc comparisons). PGR absorbance was measured immediately after the addition of $ONOO^-$. (C) PPS-MS scavenge ^-OCl dose-dependently (one-way ANOVA $p < 0.001$, *significant posthoc comparisons). ^-OCl levels were measured after 10 min of exposure.

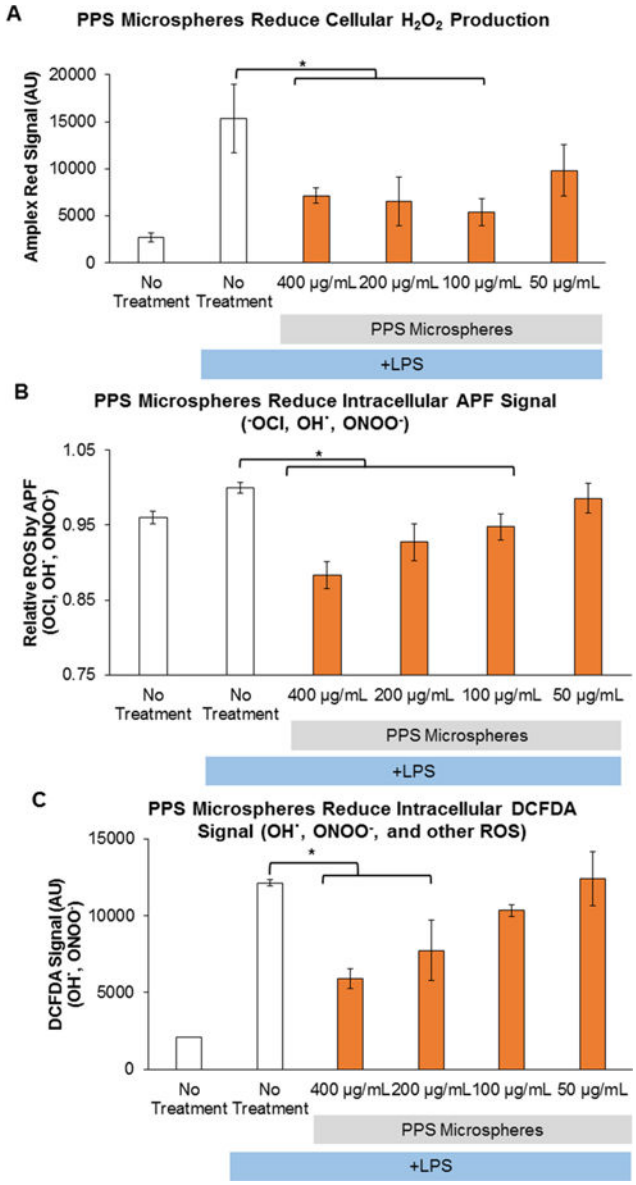

Figure 4.

PPS-MS reduce ROS in LPS-stimulated RAW macrophages. (A) PPS-MS significantly reduce secreted H_2O_2 in stimulated RAW macrophages measured by Amplex Red (one-way ANOVA $p < 0.05$, *significant posthoc comparison). (B) PPS-MS scavenge intracellular $^{-}$OCl and other ROS in a dose-dependent manner (one-way ANOVA $p < 0.05$, *significant posthoc comparisons). (C) PPS-MS reduce multiple ROS species as measured by DCFDA, and the response is dose dependent (one-way ANOVA $p < 0.05$, *significant posthoc comparisons). In all cell experiments, RAW macrophages were treated for 1 h with PPS-MS followed by the addition of LPS. After 24 h of incubation with PPS-MS and LPS, ROS levels were measured. Data presented as mean ± SD.

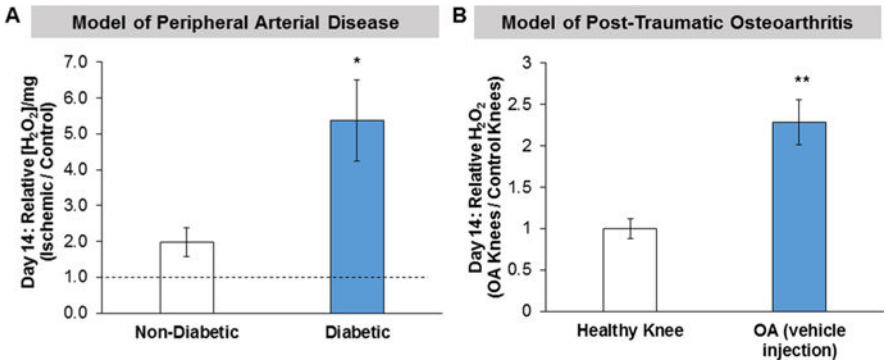

Figure 5.

H_2O_2, measured with Amplex Red, is elevated in two disease models of injury. (A) Tissue H_2O_2 levels in ischemic gastrocnemius muscles excised from diabetic and age-matched nondiabetic mice. The mice with 15 weeks of diabetes had a greater increase in relative H_2O_2 levels in the gastrocnemius muscle compared to nondiabetic mice. Additionally, H_2O_2 was elevated in the ischemic limb relative to the control limb (ischemic/control ratio >1) in both the nondiabetic and diabetic mice. $n = 4–5$ mice/group. $*p < 0.05$ for nondiabetic vs diabetic mice. (B) Tissue H_2O_2 levels in knee joints from mice with and without load-induced osteoarthritis. H_2O_2 levels were significantly elevated in knees with OA compared to healthy knees. $n = 6$ knees/group (3 mice), mean ± SD, $**p < 0.01$ for OA vs healthy knees.

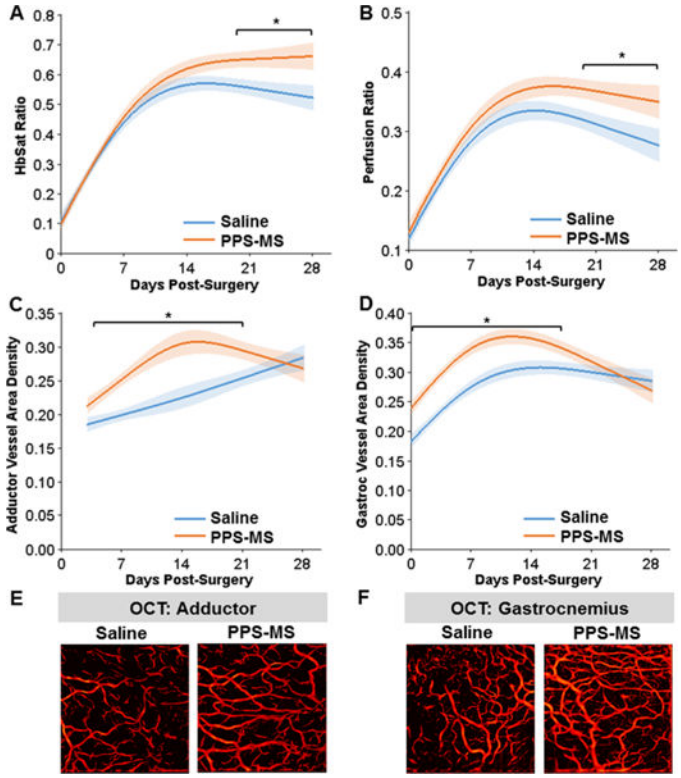

Figure 6.

HbSat, perfusion, and vessel density were increased in the ischemic limb of diabetic mice treated with PPS-MS. (A) Analysis of the GLM curves for the HbSat response showed a significantly greater HbSat ratio for the PPS-MS treated group for days 19–28. (B) Analysis of the GLM curves for the perfusion ratio showed a significant difference between the two treatment groups for days 19–28. (C–F) Vessel morphology parameters were quantified from OCT images of the adductor and gastrocnemius muscle regions. Analysis of the GLM curves for vessel area density shows that the two groups differ significantly (C) from days 4–21 in the adductor and (D) from days 0–17 in the gastrocnemius. (E, F) OCT images of the vasculature from Day 7 (images are projections of all vessels present in a volume acquired over a 4 mm × 4 mm area). (*$p < 0.05$, n = 17–20/group for days 0–7 and n = 6–7/group for days 14–28.).

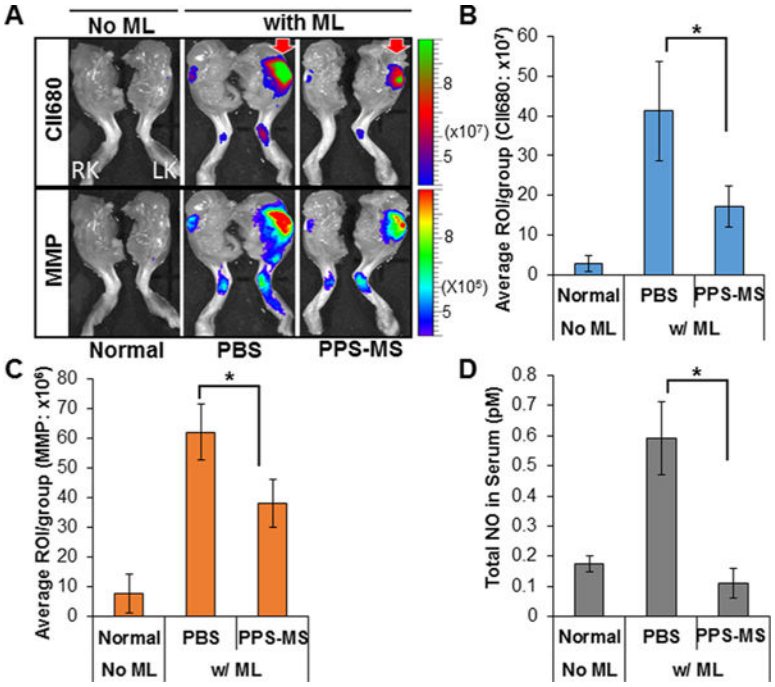

Figure 7.

PPS-MS reduce knee damage in PTOA. Mice were mechanically loaded (ML) unilaterally in the left knee and then optically imaged in vivo for binding of MabCII680 and evaluation of MMP activity 2 weeks post-initiation of injury. (A) Optical imaging of normal control mice and unilateral PTOA mice treated with PBS or PPS-MS (RK, right knee; LK, left knee). (B, C) Quantitative optical imaging of MabCII bound to damaged cartilage and MMP activity in left knee joint shows significant decreases with PPS-MS treatment. (D) PPS-MS have an inhibitory effect on total NO production in the PTOA mouse model, as shown by levels of total NO measured in sera of treated mice 2 weeks postinitiation of injury. (Data are expressed as mean ± SD, $*p < 0.05$, $n = 6$/group.)